A Hierarchy of Models for Microgrids With Grid-Feeding Inverters

Olaolu Ajala*, Murilo Almeida†, Ivan Celanovic†, Peter Sauer*, and Alejandro Domínguez-García*
*Department of Electrical and Computer Engineering
University of Illinois at Urbana Champaign
306 N Wright St, Urbana, IL 61801 USA
Email: {ooajala2, psauer, aledan}@illinois.edu
†Typhoon HIL, Inc., 35 Medford St. Suite 305, Somerville, MA 02143
Email: {murilo.almeida, ivanc}@typhoon-hil.com

***Abstract*—This work develops a hierarchy of models, each with distinct time resolutions, for microgrids having grid-feeding inverters at all generation buses. Specifically, our focus is on microgrids with battery storage units connected to an electrical network via grid-feeding inverters. The process of developing the model hierarchy involves three key stages: (1) the formulation of a microgrid high-order model using circuit-theoretic and control laws, (2) the systematic reduction of this high-order model to distinct reduced-order models using singular perturbation techniques, and (3) an identification of the time resolutions for which each reduced-order model is valid. A comparison between the responses of all the models developed and that of a microgrid ultra-high fidelity model is presented.**

I. Introduction

A microgrid may be defined as a collection of loads and distributed energy resources (DERs), interconnected via an electrical network with a small physical footprint, which is capable of operating in (1) grid-connected mode, as part of a large power system; or (2) islanded mode, as an autonomous power system. The DERs that constitute a microgrid are often interfaced to the electrical network via a grid-feeding inverter, where the real and reactive power injections are controlled to track a given reference; or via a grid-forming inverter, where the output voltage magnitude and frequency are controlled to track a given reference.

As the popularity and adoption of the microgrid concept in electricity systems increases, it becomes necessary to develop comprehensive mathematical models. Models are tools that control engineers, scientists, mathematicians, and other non experts in the field of microgrids, require for the different analysis and control design tasks necessary for development of innovative microgrid technologies. Accurate mathematical models may be developed for inverter-based microgrids by utilizing concepts from circuit-theoretic and control theory. However, the resulting models are often highly complex and too detailed for the particular application. It therefore becomes necessary to simplify these models to less detailed ones which, though less accurate, can represent the phenomena relevant to the application of interest.

The main contribution of this paper is the development of a time-resolution-based hierarchy of models for inverter-based microgrids, and an identification of the time resolution for which each model is valid. The focus of this work is on microgrids with power supplies connected to an electrical network via grid-feeding inverters. Using Kirchhoff's laws, component terminal relations, and basic control law definitions, a microgrid high-order model (μHOm) is developed. Afterwards, two reduced-order models, referred to as microgrid reduced-order model 1 (μROm1) and microgrid reduced-order model 2 (μROm2), are obtained from the μHOm using singular perturbation techniques for model-order reduction. The time resolution for which the reduced-order models are valid is identified, and all three models are explicitly presented with the small parameters used for singular perturbation analysis identified. Finally, for some test cases, the responses of all three models are compared to that of a microgrid ultra-high fidelity model (UHΦm) that is: (1) designed to mimic a real system, and (2) modeled on a real-time simulator platform developed by Typhoon HIL, Inc. [1].

The development of mathematical models for microgrids with grid-feeding inverters has received significant

*The information, data, or work presented herein was supported by the Advanced Research Projects Agency-Energy (ARPA-E), U.S. Department of Energy, within the NODES program, under Award DE-AR0000695.

attention in the research community. Recent work in this area includes formulations of (1) switched models, referred to as the UHΦm in this work, which are very detailed and capture the high frequency switching transients introduced by the inverter Pulse Width Modulation (PWM) mechanism [15], (2) averaged models, referred to as the μHOm in this work, which are slightly less elaborate and describe dynamics of the average values of variables, neglecting the PWM switching transients [15], and (3) reduced-order models, referred to as μROm2 in this paper, which approximate the inverter-interfaced power supply with a constant power source. Although the formulations of these models are usually detailed, authors fail to identify the time resolutions associated with the different models. More specifically, Pogaku et al. [11] presents a high-order model for grid-forming-inverter based microgrids but exclude a discussion on model-order reduction. Anand and Fernandes [3], and Rasheduzzaman et al. [12] present reduced-order models for microgrids but the models are obtained using small-signal analysis, which is only valid within certain operating regions. Kodra et al. [7] discuss the model-order reduction of an islanded microgrid using singular perturbation analysis. However, the electrical network dynamics are not included in the high-order model presented, and a simple linear model, which does not fully capture the dynamics of the islanded microgrid, is used for the singular perturbation analysis. Schiffer et al. [14] develop a detailed high-order model for grid-feeding-inverter-based microgrids, and singular perturbation analysis is employed to perform time-scale separation and model-order reduction with the underlying assumptions stated. However, though the authors claim that the model-order reduction can be performed, the small parameters in the model used for singular perturbation analysis are not explicitly identified, and details of the singular perturbation analysis are not presented. Also, just one reduced-order model is developed, and the time resolution associated with the model is not identified.

II. Preliminaries

In this section, we first introduce the $qd0$ transformation of three-phase variables to arbitrary and synchronous reference frames. Next, we introduce graph-theoretic notions used in later developments to develop the microgrid network model. Finally, a primer on singular perturbation analysis for model-order reduction is presented.

A. The $qd0$ Transformation

Let $\alpha(t)$ denote the angular position of a reference frame rotating at an arbitrary angular velocity, $\omega(t)$, and let $\mathbf{f}_{qd0[\alpha(t)]}(t) = \begin{bmatrix} f_{q[\alpha(t)]}(t) & f_{d[\alpha(t)]}(t) & f_{0[\alpha(t)]}(t) \end{bmatrix}^{\mathrm{T}}$ denote the $qd0$ transform of a vector of 3-phase variables, $\mathbf{f}_{abc}(t) = \begin{bmatrix} f_a(t) & f_b(t) & f_c(t) \end{bmatrix}^{\mathrm{T}}$, to the reference frame. The general form of the non-power-invariant $qd0$ transformation is given by:

$$\mathbf{f}_{qd0[\alpha(t)]}(t) = \mathbf{K}_1(\alpha(t))\mathbf{f}_{abc}(t), \tag{1}$$

where:

$$\mathbf{K}_1(\alpha(t)) = \frac{2}{3}\begin{bmatrix} \cos(\alpha(t)) & \cos(\alpha(t)-\frac{2\pi}{3}) & \cos(\alpha(t)+\frac{2\pi}{3}) \\ \sin(\alpha(t)) & \sin(\alpha(t)-\frac{2\pi}{3}) & \sin(\alpha(t)+\frac{2\pi}{3}) \\ \frac{1}{2} & \frac{1}{2} & \frac{1}{2} \end{bmatrix},$$

$$\alpha(t) = \int_0^t \omega(\tau)\, d\tau + \alpha(0).$$

The $qd0$ reference frame in (1) is referred to as the arbitrary reference frame, but when $\alpha(t) = \omega_0 t$, where ω_0 denotes the synchronous frequency, it is referred to as the synchronously rotating reference frame [9].

Assume that $f_a(t)$, $f_b(t)$, and $f_c(t)$ are a balanced three-phase set. Let $\overrightarrow{\mathbf{f}}_{qd0[\omega_0 t]}(t)$ and $\overrightarrow{\mathbf{f}}_{qd0[\alpha(t)]}(t)$ denote the complex representation of $\mathbf{f}_{abc}(t)$ in the synchronously rotating reference frame and the arbitrary reference frame, respectively. Then, by using (1), we have that for

$$\overrightarrow{\mathbf{f}}_{qd0[\cdot]}(t) := f_{q[\cdot]}(t) - \mathrm{j} f_{d[\cdot]}(t), \tag{2}$$

where j denotes the complex variable, i.e., $\mathrm{j} = \sqrt{-1}$,

$$\overrightarrow{\mathbf{f}}_{qd0[\alpha(t)]}(t) = \overrightarrow{\mathbf{f}}_{qd0[\omega_0 t]}(t)\exp(-\mathrm{j}\delta(t)), \tag{3}$$

with

$$\delta(t) := \alpha(t) - \omega_0 t.$$

[Note that because of the balanced assumption on $f_a(t)$, $f_b(t)$, and $f_c(t)$, $f_{0[\alpha(t)]}(t) = 0$.]

Let $\hat{\mathbf{f}}_{qd0[\alpha(t)]}(t) = \begin{bmatrix} f_{q[\alpha(t)]}(t) & f_{d[\alpha(t)]}(t) \end{bmatrix}^{\mathrm{T}}$, and $\hat{\mathbf{f}}_{qd0[\omega_0 t]}(t) = \begin{bmatrix} f_{q[\omega_0 t]}(t) & f_{d[\omega_0 t]}(t) \end{bmatrix}^{\mathrm{T}}$; then from (2)–(3), it follows that:

$$\hat{\mathbf{f}}_{qd0[\alpha(t)]}(t) = \mathbf{K}_2(\delta(t))\hat{\mathbf{f}}_{qd0[\omega_0 t]}(t), \tag{4}$$

with

$$\mathbf{K}_2(\delta(t)) = \begin{bmatrix} \cos(\delta(t)) & -\sin(\delta(t)) \\ \sin(\delta(t)) & \cos(\delta(t)) \end{bmatrix},$$

and the evolution of $\delta(t)$ governed by:

$$\frac{d\delta(t)}{dt} = \omega(t) - \omega_0. \tag{5}$$

B. Graph-Theoretic Network Model

The topology of the microgrid electrical network can be described by a connected undirected graph, $\mathcal{G} = (\mathcal{V}, \mathcal{E})$, with $\mathcal{V}$ denoting the set of buses in the network, so that $\mathcal{V} := \{1, 2, \ldots, |\mathcal{V}|\}$, and $\mathcal{E} \subset \mathcal{V} \times \mathcal{V}$, so that $\{j, k\} \in \mathcal{E}$ if buses j and k are electrically connected. Choose an arbitrary orientation for each of the elements in $\mathcal{E}$; then we can define an incidence matrix, $\boldsymbol{M} = [m_{ie}] \in \mathbb{R}^{n \times |\mathcal{E}|}$, associated with this orientation as follows:

$$\begin{aligned} m_{ie} &= 1 \quad \text{if edge } e \text{ is directed away from node } i, \\ m_{ie} &= -1 \quad \text{if edge } e \text{ is directed into node } i, \\ m_{ie} &= 0 \quad \text{if edge } e \text{ is not incident on node } i. \end{aligned}$$

Connected to some buses, we assume that there is an inverter-interfaced source, the dynamics of which are described in Section III-A; and at each bus, we assume there is another element, the dynamics of which are described by a generic dynamical model satisfying some properties, as described in Section III-C.

Let $\mathcal{V}_{\mathcal{I}} \subseteq \mathcal{V}$ denote the set of buses with an inverter-interfaced source. For $j = 1, 2, \ldots, |\mathcal{V}_{\mathcal{I}}|$, let s_j be used to identify variables associated with the inverter-interfaced source connected to bus j. As a result, we can represent the resistance, inductance and current injection of the source as: $R^{(s_j)}$, $L^{(s_j)}$ and $I^{(s_j)}(t)$, respectively.

For $j = 1, 2, \ldots, |\mathcal{V}|$, let l_j be used to identify variables associated with an element connected to bus j. As a result, we can represent the resistance, inductance and current injection of the element as: $R^{(l_j)}$, $L^{(l_j)}$ and $I^{(l_j)}(t)$, respectively.

For $m = 1, 2, \ldots, |\mathcal{E}|$, let $e_m := \{j, k\}$, $\{j, k\} \in \mathcal{E}$. As a result, we can represent the resistance, inductance and current across a line extending from bus j to bus k as: $R^{(e_m)}$, $L^{(e_m)}$ and $I^{(e_m)}(t)$, respectively.

C. A Primer on Singular Perturbation Analysis

Definition (Big $\mathcal{O}$ notation)**.** *Consider a function $f(\epsilon)$, defined on some subset of the real numbers. We write $f(\epsilon) = \mathcal{O}\left(\epsilon^k\right)$ if and only if there exists a positive real number C, such that:*

$$\left|f(\epsilon)\right| \leq C\epsilon^k, \text{ as } \epsilon \to 0.$$

The material in this section follows closely from the developments in ([8], pp. 1–12) and ([6], pp. 7–11). Consider the following two-time-scale dynamical model:

$$\begin{aligned} \dot{\mathbf{x}}(t) &= f\left(\mathbf{x}(t), \mathbf{z}(t), \mathbf{w}(t), \epsilon\right), & \mathbf{x}(0) &= \mathbf{x}^0, \\ \epsilon\dot{\mathbf{z}}(t) &= g\left(\mathbf{x}(t), \mathbf{z}(t), \mathbf{w}(t), \epsilon\right), & \mathbf{z}(0) &= \mathbf{z}^0, \\ \mathbf{0} &= h\left(\mathbf{x}(t), \mathbf{z}(t), \mathbf{w}(t), \epsilon\right), & \mathbf{w}(0) &= \mathbf{w}^0, \end{aligned} \tag{6}$$

with slow and fast time-scales, t and τ, respectively, where $\tau = \frac{t}{\epsilon}$, $f(\cdot, \cdot, \cdot, \epsilon) = \mathcal{O}(1)$, $g(\cdot, \cdot, \cdot, \epsilon) = \mathcal{O}(1)$, and $h(\cdot, \cdot, \cdot, \epsilon) = \mathcal{O}(1)$.

Assumption II.1. *Let the bar ($\bar{}$) and tilde ($\tilde{}$) notations be used to describe the slow t-scale and fast τ-scale variables, respectively.* $\mathbf{x}$*,* $\mathbf{z}$ *and* $\mathbf{w}$ *can be decoupled to*

$$\begin{aligned} \mathbf{x}(t) &= \bar{\mathbf{x}}(t) + \tilde{\mathbf{x}}(\tau), \\ \mathbf{z}(t) &= \bar{\mathbf{z}}(t) + \tilde{\mathbf{z}}(\tau), \\ \mathbf{w}(t) &= \bar{\mathbf{w}}(t) + \tilde{\mathbf{w}}(\tau), \end{aligned}$$

where

$$\begin{aligned} \bar{\mathbf{x}}(t) &= \bar{\mathbf{x}}_{\mathbf{0}}(t) + \epsilon\bar{\mathbf{x}}_{\mathbf{1}}(t) + \epsilon^2\bar{\mathbf{x}}_{\mathbf{2}}(t) + \cdots, \\ \tilde{\mathbf{x}}(\tau) &= \tilde{\mathbf{x}}_{\mathbf{0}}(\tau) + \epsilon\tilde{\mathbf{x}}_{\mathbf{1}}(\tau) + \epsilon^2\tilde{\mathbf{x}}_{\mathbf{2}}(\tau) + \cdots, \\ \bar{\mathbf{z}}(t) &= \bar{\mathbf{z}}_{\mathbf{0}}(t) + \epsilon\bar{\mathbf{z}}_{\mathbf{1}}(t) + \epsilon^2\bar{\mathbf{z}}_{\mathbf{2}}(t) + \cdots, \\ \tilde{\mathbf{z}}(\tau) &= \tilde{\mathbf{z}}_{\mathbf{0}}(\tau) + \epsilon\tilde{\mathbf{z}}_{\mathbf{1}}(\tau) + \epsilon^2\tilde{\mathbf{z}}_{\mathbf{2}}(\tau) + \cdots, \\ \bar{\mathbf{w}}(t) &= \bar{\mathbf{w}}_{\mathbf{0}}(t) + \epsilon\bar{\mathbf{w}}_{\mathbf{1}}(t) + \epsilon^2\bar{\mathbf{w}}_{\mathbf{2}}(t) + \cdots, \\ \tilde{\mathbf{w}}(\tau) &= \tilde{\mathbf{w}}_{\mathbf{0}}(\tau) + \epsilon\tilde{\mathbf{w}}_{\mathbf{1}}(\tau) + \epsilon^2\tilde{\mathbf{w}}_{\mathbf{2}}(\tau) + \cdots. \end{aligned}$$

The dynamical model in (6) may be rewritten in terms of t and τ as:

$$\begin{aligned} \dot{\bar{\mathbf{x}}}(t) + \frac{1}{\epsilon}\frac{d\tilde{\mathbf{x}}(\tau)}{d\tau} &= f\left(\bar{\mathbf{x}}(t) + \tilde{\mathbf{x}}(\tau), \bar{\mathbf{z}}(t) + \tilde{\mathbf{z}}(\tau), \bar{\mathbf{w}}(t) + \tilde{\mathbf{w}}(\tau), \epsilon\right), \\ \epsilon\dot{\bar{\mathbf{z}}}(t) + \frac{d\tilde{\mathbf{z}}(\tau)}{d\tau} &= g\left(\bar{\mathbf{x}}(t) + \tilde{\mathbf{x}}(\tau), \bar{\mathbf{z}}(t) + \tilde{\mathbf{z}}(\tau), \bar{\mathbf{w}}(t) + \tilde{\mathbf{w}}(\tau), \epsilon\right), \\ \mathbf{0} &= h\left(\bar{\mathbf{x}}(t) + \tilde{\mathbf{x}}(\tau), \bar{\mathbf{z}}(t) + \tilde{\mathbf{z}}(\tau), \bar{\mathbf{w}}(t) + \tilde{\mathbf{w}}(\tau), \epsilon\right), \end{aligned}$$

and by setting $\epsilon = 0$, it follows that:

$$\begin{aligned} &\frac{d\tilde{\mathbf{x}}_0(\tau)}{d\tau} = 0, \\ &\dot{\bar{\mathbf{x}}}_0(t) = f\left(\bar{\mathbf{x}}_0(t) + \tilde{\mathbf{x}}_{\mathbf{0}}(\infty), \bar{\mathbf{z}}_0(t) + \tilde{\mathbf{z}}_0(\infty), \bar{\mathbf{w}}_0(t) + \tilde{\mathbf{w}}_0(\infty), 0\right), \\ &\frac{d\tilde{\mathbf{z}}_0(\tau)}{d\tau} = g\left(\bar{\mathbf{x}}_0(0) + \tilde{\mathbf{x}}_{\mathbf{0}}(\tau), \bar{\mathbf{z}}_0(0) + \tilde{\mathbf{z}}_0(\tau), \bar{\mathbf{w}}_0(0) + \tilde{\mathbf{w}}_0(\tau), 0\right), \end{aligned}$$

and

$$\begin{aligned} \mathbf{0} &= h\left(\bar{\mathbf{x}}_0(0) + \tilde{\mathbf{x}}_{\mathbf{0}}(\tau), \bar{\mathbf{z}}_0(0) + \tilde{\mathbf{z}}_0(\tau), \bar{\mathbf{w}}_0(0) + \tilde{\mathbf{w}}_0(\tau), 0\right), \\ \mathbf{0} &= h\left(\bar{\mathbf{x}}_0(t) + \tilde{\mathbf{x}}_{\mathbf{0}}(\infty), \bar{\mathbf{z}}_0(t) + \tilde{\mathbf{z}}_0(\infty), \bar{\mathbf{w}}_0(t) + \tilde{\mathbf{w}}_0(\infty), 0\right). \end{aligned} \tag{7}$$

Assumption II.2. *Equation* (7) *has distinct real roots, one of which is:*

$$\begin{aligned} \bar{\mathbf{w}}_0(0) + \tilde{\mathbf{w}}_0(\tau) &= \nu\left(\bar{\mathbf{x}}_0(0) + \tilde{\mathbf{x}}_{\mathbf{0}}(\tau), \bar{\mathbf{z}}_0(0) + \tilde{\mathbf{z}}_0(\tau)\right), \\ \bar{\mathbf{w}}_0(t) + \tilde{\mathbf{w}}_0(\infty) &= \nu\left(\bar{\mathbf{x}}_0(t) + \tilde{\mathbf{x}}_{\mathbf{0}}(\infty), \bar{\mathbf{z}}_0(t) + \tilde{\mathbf{z}}_0(\infty)\right). \end{aligned}$$

Choosing initial conditions $\tilde{\mathbf{x}}_0(0) = 0$ and $\bar{\mathbf{x}}_0(0) = \mathbf{x}^0$, let $\bar{\mathbf{z}}_0(t) = \zeta\left(\bar{\mathbf{x}}_0(t)\right)$ be a root of

$$\mathbf{0} = g\left(\bar{\mathbf{x}}_0(t), \bar{\mathbf{z}}_0(t), \nu\left(\bar{\mathbf{x}}_0(t), \bar{\mathbf{z}}_0(t)\right), 0\right). \tag{8}$$

As a result, the two-time-scale dynamical model in (6) may be expressed in the approximate form:

$$\dot{\bar{\mathbf{x}}}_0(t) = f\left(\bar{\mathbf{x}}_0(t), \zeta(\bar{\mathbf{x}}_0(t)), \nu\left(\bar{\mathbf{x}}_0(t), \zeta(\bar{\mathbf{x}}_0(t))\right), 0\right), \tag{9}$$

and

$$\frac{d\tilde{\mathbf{z}}_0(\tau)}{d\tau} = g\left(\mathbf{x}^0, \zeta(\mathbf{x}^0) + \tilde{\mathbf{z}}_0(\tau), \nu(\mathbf{x}^0, \zeta(\mathbf{x}^0) + \tilde{\mathbf{z}}_0(\tau)), 0\right), \tag{10}$$

where $\bar{\mathbf{x}}_0(0) = \mathbf{x}^0$ and $\tilde{\mathbf{z}}_0(0) = \mathbf{z}^0 - \zeta(\mathbf{x}^0)$

Assumption II.3. *The equilibrium $\tilde{\mathbf{z}}_0(\tau) = \mathbf{0}$ of* (10) *is asymptotically stable in $\mathbf{x}^0$, and $\tilde{\mathbf{z}}_0(0)$ belongs to its domain of attraction.*

Assumption II.4. *The eigenvalues of $\frac{\partial g}{\partial \mathbf{z}}$ (the Jacobian of* (8)*) evaluated, for $\epsilon = 0$, along $\bar{\mathbf{x}}_0(t)$, $\bar{\mathbf{z}}_0(t)$, have real parts smaller than a fixed negative number.*

Theorem (Tikhonov's theorem)**.** *Let f and g in* (6) *be sufficiently many times continuously differentiable functions of their arguments, and let the root, $\bar{\mathbf{z}}_0(t) = \zeta\left(\bar{\mathbf{x}}_0(t)\right)$ of* (8) *be distinct and real, in the domain of interest. Then, if assumptions II.1, II.2, II.3 and II.4 are satisfied,* (6) *can be approximated by* (9) *and* (10)*, where*

$$\begin{aligned}
\mathbf{x}(t) &= \bar{\mathbf{x}}_0(t) + \mathcal{O}(\epsilon),\\
\mathbf{z}(t) &= \zeta(\bar{\mathbf{x}}_0(t)) + \tilde{\mathbf{z}}_0(\tau) + \mathcal{O}(\epsilon),\\
\mathbf{w}(t) &= \nu\left(\bar{\mathbf{x}}_0(t), \zeta(\bar{\mathbf{x}}_0(t)) + \tilde{\mathbf{z}}_0(\tau)\right) + \mathcal{O}(\epsilon),
\end{aligned}$$

and there exists $t_0 > 0$ such that

$$\begin{aligned}
\mathbf{z}(t) &= \zeta(\bar{\mathbf{x}}_0(t)) + \mathcal{O}(\epsilon),\\
\mathbf{w}(t) &= \nu\left(\bar{\mathbf{x}}_0(t), \zeta(\bar{\mathbf{x}}_0(t))\right) + \mathcal{O}(\epsilon),
\end{aligned}$$

for all $t > t_0$.

> In this work, we refer to the approximate slow component in (9) as the reduced-order model.

Definition (Time resolution)**.** *The time-resolution of the reduced-order model in* (9) *is the time it takes the approximate fast component in* (10) *to reach the equilibrium $\tilde{\mathbf{z}}_0(\tau) = \mathbf{0}$ from an initial state $\tilde{\mathbf{z}}_0(0) = \mathbf{z}^0 - \zeta(\mathbf{x}^0)$.*

Consider the dynamical model in (6). If we choose ϵ such that $-\frac{1}{\epsilon}$ is greater than the real part of eigenvalues associated with the fast dynamics, then the fast model in (10) reaches equilibrium $\tilde{\mathbf{z}}_0(\tau) = \mathbf{0}$ in around 5ϵ seconds. As a result, we say that the time resolution of the reduced-order model in (9) is 5ϵ seconds.

III. Microgrid High-Order Model

In this section, basic circuit laws are used in conjunction with notions introduced in Section II to develop a High-Order model for a grid-feeding-inverter-based AC microgrid operating in grid-connected mode. First, a model is developed for an inverter-interfaced source, which includes a battery, a 3-phase inverter, an LCL filter, an outer power controller and inner current controller, and a phase-locked loop. Next, a three-phase model for the electrical network is developed, along with a generic model for an element (typically a load) connected between each bus and the ground.

The Microgrid High-Order Model (μHOm), whose system model is depicted in Fig. 1 below, is developed by combining the inverter-interfaced source model, the network model and the generic element model. In this work, the models developed are expressed using the per-unit representation, to ease analysis in later developments.

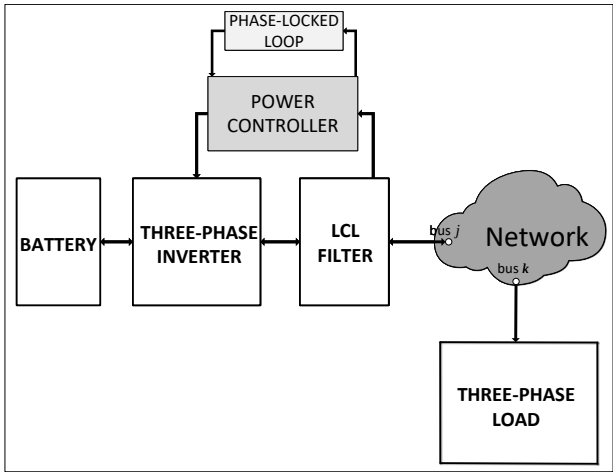

Fig. 1: Microgrid Model.

A. Inverter-Interfaced Source Model

The structure of the inverter-interfaced source adopted in this work, shown in Fig. 1, is comprised of a 3-phase inverter coupled with a battery, an LCL filter, a power controller and a phase-locked loop (PLL). An averaged model, as opposed to a switched model, is used to describe the 3-phase inverter dynamics (see [15], pp. 27–38, for more details).

For the inverter connected to bus j of the microgrid network, let $V_{DC}^{(s_j)}$ denote the dc voltage at the inverter input. Let $U^{(s_j)}(t)$, $E^{(s_j)}(t)$, $\hat{E}^{(s_j)}(t)$ and $V^{(s_j)}(t)$ denote the Pulse Width Modulation (PWM) output voltage of the inverter, the internal voltage of the inverter, the LCL filter capacitor voltage, and the voltage at bus j, in per-unit representation, respectively. Let $\Xi^{(s_j)}(t)$ and $I^{(s_j)}(t)$ denote the inverter output current and the filtered inverter output current, in per-unit representation, respectively. Let $\Gamma^{(s_j)}(t)$ denote the state variable for the current controller, in per-unit representation. Let $\boldsymbol{P}_r^{(s_j)}$ and $\boldsymbol{Q}_r^{(s_j)}$ denote the inverter three-phase real and reactive power references, in per-unit representation,

respectively. Let $\Lambda^{(s_j)}(t)$ denote the state variable for the phase-locked loop (PLL), in per-unit representation. Then, using the $qd0$ transformation discussed in Section II, the dynamics of the inverter-interfaced source connected to bus j of the microgrid electrical network can be described by:

$$
\begin{aligned}
\frac{1}{\omega_0}\frac{d\delta^{(s_j)}(t)}{dt} &= -K_{P\lambda}^{(s_j)}E_{d[\alpha^{(j)}(t)]}^{(s_j)}(t) + K_{I\lambda}^{(s_j)}\Lambda_{[\alpha^{(j)}(t)]}^{(s_j)}(t) - 1,\\
\frac{L^{(s_j)}}{\omega_0}\frac{dI_{q[\omega_0 t]}^{(s_j)}(t)}{dt} &= -R^{(s_j)}I_{q[\omega_0 t]}^{(s_j)}(t) - L^{(s_j)}I_{d[\omega_0 t]}^{(s_j)}(t) + E_{q[\omega_0 t]}^{(s_j)}(t)\\
&\quad - V_{q[\omega_0 t]}^{(l_j)}(t),\\
\frac{L^{(s_j)}}{\omega_0}\frac{dI_{d[\omega_0 t]}^{(s_j)}(t)}{dt} &= L^{(s_j)}I_{q[\omega_0 t]}^{(s_j)}(t) - R^{(s_j)}I_{d[\omega_0 t]}^{(s_j)}(t) + E_{d[\omega_0 t]}^{(s_j)}(t)\\
&\quad - V_{d[\omega_0 t]}^{(l_j)}(t),\\
\frac{C^{(s_j)}}{\omega_0}\frac{d\hat{E}_{q[\omega_0 t]}^{(s_j)}(t)}{dt} &= -I_{q[\omega_0 t]}^{(s_j)}(t) - C^{(s_j)}\hat{E}_{d[\omega_0 t]}^{(s_j)}(t) + \Xi_{q[\omega_0 t]}^{(s_j)}(t),\\
\frac{C^{(s_j)}}{\omega_0}\frac{d\hat{E}_{d[\omega_0 t]}^{(s_j)}(t)}{dt} &= -I_{d[\omega_0 t]}^{(s_j)}(t) + C^{(s_j)}\hat{E}_{q[\omega_0 t]}^{(s_j)}(t) + \Xi_{d[\omega_0 t]}^{(s_j)}(t),\\
\frac{L_0^{(s_j)}}{\omega_0}\frac{d\Xi_{q[\alpha^{(j)}(t)]}^{(s_j)}(t)}{dt} &= \frac{V_{DC}^{(s_j)}K_{I\gamma}^{(s_j)}}{2}\Gamma_{q[\alpha^{(j)}(t)]}^{(s_j)}(t)\\
&\quad - \left(R_0^{(s_j)} + \frac{V_{DC}^{(s_j)}K_{P\gamma}^{(s_j)}}{2}\right)\Xi_{q[\alpha^{(j)}(t)]}^{(s_j)}(t)\\
&\quad + \frac{V_{DC}^{(s_j)}K_{P\gamma}^{(s_j)}}{2}\frac{\boldsymbol{P}_r^{(s_j)}E_{q[\alpha^{(j)}(t)]}^{(s_j)}(t) - \boldsymbol{Q}_r^{(s_j)}E_{d[\alpha^{(j)}(t)]}^{(s_j)}(t)}{E_{q[\alpha^{(j)}(t)]}^{(s_j)}(t)^2 + E_{d[\alpha^{(j)}(t)]}^{(s_j)}(t)^2},\\
\frac{L_0^{(s_j)}}{\omega_0}\frac{d\Xi_{d[\alpha^{(j)}(t)]}^{(s_j)}(t)}{dt} &= \frac{V_{DC}^{(s_j)}K_{I\gamma}^{(s_j)}}{2}\Gamma_{d[\alpha^{(j)}(t)]}^{(s_j)}(t)\\
&\quad - \left(R_0^{(s_j)} + \frac{V_{DC}^{(s_j)}K_{P\gamma}^{(s_j)}}{2}\right)\Xi_{d[\alpha^{(j)}(t)]}^{(s_j)}(t)\\
&\quad + \frac{V_{DC}^{(s_j)}K_{P\gamma}^{(s_j)}}{2}\frac{\boldsymbol{P}_r^{(s_j)}E_{d[\alpha^{(j)}(t)]}^{(s_j)}(t) + \boldsymbol{Q}_r^{(s_j)}E_{q[\alpha^{(j)}(t)]}^{(s_j)}(t)}{E_{q[\alpha^{(j)}(t)]}^{(s_j)}(t)^2 + E_{d[\alpha^{(j)}(t)]}^{(s_j)}(t)^2},\\
E_{q[\alpha^{(j)}(t)]}^{(s_j)}(t) &= \left(-I_{q[\alpha^{(j)}(t)]}^{(s_j)}(t) + \Xi_{q[\alpha^{(j)}(t)]}^{(s_j)}(t)\right)\hat{R}_0^{(s_j)}\\
&\quad + \hat{E}_{q[\alpha^{(j)}(t)]}^{(s_j)}(t),\\
E_{d[\alpha^{(j)}(t)]}^{(s_j)}(t) &= \left(-I_{d[\alpha^{(j)}(t)]}^{(s_j)}(t) + \Xi_{d[\alpha^{(j)}(t)]}^{(s_j)}(t)\right)\hat{R}_0^{(s_j)}\\
&\quad + \hat{E}_{d[\alpha^{(j)}(t)]}^{(s_j)}(t),\\
\hat{\mathbf{E}}_{qd0[\alpha^{(j)}(t)]}(t) &= \mathbf{K}_2(\delta^{(s_j)}(t))\hat{\mathbf{E}}_{qd0[\omega_0 t]}(t),\\
\hat{\boldsymbol{\Xi}}_{qd0[\alpha^{(j)}(t)]}(t) &= \mathbf{K}_2(\delta^{(s_j)}(t))\hat{\boldsymbol{\Xi}}_{qd0[\omega_0 t]}(t),\\
\frac{1}{\omega_0}\frac{d\Gamma_{q[\alpha^{(j)}(t)]}^{(s_j)}(t)}{dt} &= \frac{\boldsymbol{P}_r^{(s_j)}E_{q[\alpha^{(j)}(t)]}^{(s_j)}(t) - \boldsymbol{Q}_r^{(s_j)}E_{d[\alpha^{(j)}(t)]}^{(s_j)}(t)}{E_{q[\alpha^{(j)}(t)]}^{(s_j)}(t)^2 + E_{d[\alpha^{(j)}(t)]}^{(s_j)}(t)^2}\\
&\quad - \Xi_{q[\alpha^{(j)}(t)]}^{(s_j)}(t),\\
\frac{1}{\omega_0}\frac{d\Gamma_{d[\alpha^{(j)}(t)]}^{(s_j)}(t)}{dt} &= \frac{\boldsymbol{P}_r^{(s_j)}E_{d[\alpha^{(j)}(t)]}^{(s_j)}(t) + \boldsymbol{Q}_r^{(s_j)}E_{q[\alpha^{(j)}(t)]}^{(s_j)}(t)}{E_{q[\alpha^{(j)}(t)]}^{(s_j)}(t)^2 + E_{d[\alpha^{(j)}(t)]}^{(s_j)}(t)^2}\\
&\quad - \Xi_{d[\alpha^{(j)}(t)]}^{(s_j)}(t),\\
\frac{1}{\omega_0}\frac{d\Lambda_{[\alpha^{(j)}(t)]}^{(s_j)}(t)}{dt} &= -E_{d[\alpha^{(j)}(t)]}^{(s_j)}(t).
\end{aligned}
\tag{11}
$$

where $L_0^{(s_j)}$, $L^{(s_j)}$ and $C^{(s_j)}$ denote the inductances and capacitance of the LCL filter, in per-unit representation, respectively; $R_0^{(s_j)}$, $\hat{R}_0^{(s_j)}$ and $R^{(s_j)}$ denote the inverter and filter resistances, in per-unit representation, respectively; $K_{P\gamma}^{(s_j)}$ and $K_{I\gamma}^{(s_j)}$ denote the proportional and integral control gains for the current controller, in per-unit representation, respectively; $K_{P\lambda}^{(s_j)}$ and $K_{I\lambda}^{(s_j)}$ denote the proportional and integral controller gains for the PLL, in per-unit representation, respectively. Filtered real and reactive power measurements, $P_f^{(s_j)}(t)$ and $Q_f^{(s_j)}(t)$, can be described by:

$$
\begin{aligned}
\frac{1}{\omega_c^{(s_j)}}\frac{dP_f^{(s_j)}(t)}{dt} &= -P_f^{(s_j)}(t) + E_{q[\omega_0 t]}^{(s_j)}(t)I_{q[\omega_0 t]}^{(s_j)}(t) + E_{d[\omega_0 t]}^{(s_j)}(t)I_{d[\omega_0 t]}^{(s_j)}(t),\\
\frac{1}{\omega_c^{(s_j)}}\frac{dQ_f^{(s_j)}(t)}{dt} &= -Q_f^{(s_j)}(t) + E_{q[\omega_0 t]}^{(s_j)}(t)I_{d[\omega_0 t]}^{(s_j)}(t) - E_{d[\omega_0 t]}^{(s_j)}(t)I_{q[\omega_0 t]}^{(s_j)}(t),
\end{aligned}
$$

with $\omega_c^{(s_j)}$ denoting the filter cut-off frequency.

B. Network Model

Assumption III.1. *All lines connecting the network buses can be represented using the short transmission line model [5].*

Let $V_{q[\omega_0 t]}^{(l_j)}(t) - \mathrm{j}V_{d[\omega_0 t]}^{(l_j)}(t)$ denote the per-unit voltage at bus j, and let $R^{(e_m)}$, $L^{(e_m)}$ and $I_{q[\omega_0 t]}^{(e_m)}(t) - \mathrm{j}I_{d[\omega_0 t]}^{(e_m)}(t)$ denote the per-unit resistance, inductance and current across line (j,k), respectively, as introduced in Section II-B. Then, the voltage across a line connecting bus j and bus k of the network can be described by:

$$
\begin{aligned}
V_{q[\omega_0 t]}^{(l_j)}(t) - V_{q[\omega_0 t]}^{(l_k)}(t) &= \frac{L^{(e_m)}}{\omega_0}\frac{dI_{q[\omega_0 t]}^{(e_m)}(t)}{dt} + R^{(e_m)}I_{q[\omega_0 t]}^{(e_m)}(t) + L^{(e_m)}I_{d[\omega_0 t]}^{(e_m)}(t),\\
V_{d[\omega_0 t]}^{(l_j)}(t) - V_{d[\omega_0 t]}^{(l_k)}(t) &= \frac{L^{(e_m)}}{\omega_0}\frac{dI_{d[\omega_0 t]}^{(e_m)}(t)}{dt} + R^{(e_m)}I_{d[\omega_0 t]}^{(e_m)}(t) - L^{(e_m)}I_{q[\omega_0 t]}^{(e_m)}(t).
\end{aligned}
$$

Let

$$
\begin{aligned}
\mathbf{V}_{q[\omega_0 t]}^{(\boldsymbol{\mathcal{V}})}(t) &= \begin{bmatrix} V_{q[\omega_0 t]}^{(l_1)}(t) & V_{q[\omega_0 t]}^{(l_2)}(t) & \cdots & V_{q[\omega_0 t]}^{(l_{|\mathcal{V}|})}(t)\end{bmatrix}^{\mathrm{T}},\\
\mathbf{V}_{d[\omega_0 t]}^{(\boldsymbol{\mathcal{V}})}(t) &= \begin{bmatrix} V_{d[\omega_0 t]}^{(l_1)}(t) & V_{d[\omega_0 t]}^{(l_2)}(t) & \cdots & V_{d[\omega_0 t]}^{(l_{|\mathcal{V}|})}(t)\end{bmatrix}^{\mathrm{T}},\\
\mathbf{I}_{q[\omega_0 t]}^{(\boldsymbol{\mathcal{E}})}(t) &= \begin{bmatrix} I_{q[\omega_0 t]}^{(e_1)}(t) & I_{q[\omega_0 t]}^{(e_2)}(t) & \cdots & I_{q[\omega_0 t]}^{(e_{|\mathcal{E}|})}(t)\end{bmatrix}^{\mathrm{T}},\\
\mathbf{I}_{d[\omega_0 t]}^{(\boldsymbol{\mathcal{E}})}(t) &= \begin{bmatrix} I_{d[\omega_0 t]}^{(e_1)}(t) & I_{d[\omega_0 t]}^{(e_2)}(t) & \cdots & I_{d[\omega_0 t]}^{(e_{|\mathcal{E}|})}(t)\end{bmatrix}^{\mathrm{T}}.
\end{aligned}
$$

Then the network dynamics are described by:

$$
\begin{aligned}
\frac{1}{\omega_0}\mathbf{L}^{(\boldsymbol{\mathcal{E}})}\frac{d\mathbf{I}_{q[\omega_0 t]}^{(\boldsymbol{\mathcal{E}})}(t)}{dt} &= -\mathbf{R}^{(\boldsymbol{\mathcal{E}})}\mathbf{I}_{q[\omega_0 t]}^{(\boldsymbol{\mathcal{E}})}(t) - \mathbf{L}^{(\boldsymbol{\mathcal{E}})}\mathbf{I}_{d[\omega_0 t]}^{(\boldsymbol{\mathcal{E}})}(t)\\
&\quad + \mathbf{M}^{\mathrm{T}}\mathbf{V}_{q[\omega_0 t]}^{(\boldsymbol{\mathcal{V}})}(t),\\
\frac{1}{\omega_0}\mathbf{L}^{(\boldsymbol{\mathcal{E}})}\frac{d\mathbf{I}_{d[\omega_0 t]}^{(\boldsymbol{\mathcal{E}})}(t)}{dt} &= -\mathbf{R}^{(\boldsymbol{\mathcal{E}})}\mathbf{I}_{d[\omega_0 t]}^{(\boldsymbol{\mathcal{E}})}(t) + \mathbf{L}^{(\boldsymbol{\mathcal{E}})}\mathbf{I}_{q[\omega_0 t]}^{(\boldsymbol{\mathcal{E}})}(t)\\
&\quad + \mathbf{M}^{\mathrm{T}}\mathbf{V}_{d[\omega_0 t]}^{(\boldsymbol{\mathcal{V}})}(t).
\end{aligned}
\tag{12}
$$

with

$$
\begin{aligned}
\mathbf{R}^{(\boldsymbol{\mathcal{E}})} &= \operatorname{diag}\left(R^{(e_1)}, \quad R^{(e_2)}, \quad \cdots, \quad R^{(e_{|\mathcal{E}|})}\right),\\
\mathbf{L}^{(\boldsymbol{\mathcal{E}})} &= \operatorname{diag}\left(L^{(e_1)}, \quad L^{(e_2)}, \quad \cdots, \quad L^{(e_{|\mathcal{E}|})}\right),
\end{aligned}
$$

where $\operatorname{diag}\left(d^{(1)}, \quad d^{(2)}, \quad \cdots, \quad d^{(n)}\right)$ is a diagonal matrix with diagonal entries $d^{(1)}, d^{(2)}, \ldots, d^{(n)}$; and

M denotes the network incidence matrix as defined in Section II.

C. Generic Element Model

Let $V^{(l_j)}_{q[\omega_0 t]}(t) - \mathrm{j}V^{(l_j)}_{d[\omega_0 t]}(t)$ denote the per-unit voltage at bus j, and let $I^{(l_j)}_{q[\omega_0 t]}(t) - \mathrm{j}I^{(l_j)}_{d[\omega_0 t]}(t)$ denote the per-unit current injection by an element (typically a load) at bus j. The dynamics can be described by a generic nonlinear system of differential equations which we assume to be of the form:

$$\begin{aligned}
\mu_V^{(l_j)}\dot{V}^{(l_j)}_{q[\omega_0 t]}(t) &= q_V\big(V^{(l_j)}_{q[\omega_0 t]}(t), V^{(l_j)}_{d[\omega_0 t]}(t), I^{(l_j)}_{q[\omega_0 t]}(t), I^{(l_j)}_{d[\omega_0 t]}(t)\big),\\
\mu_V^{(l_j)}\dot{V}^{(l_j)}_{d[\omega_0 t]}(t) &= d_V\big(V^{(l_j)}_{q[\omega_0 t]}(t), V^{(l_j)}_{d[\omega_0 t]}(t), I^{(l_j)}_{q[\omega_0 t]}(t), I^{(l_j)}_{d[\omega_0 t]}(t)\big),\\
\mu_I^{(l_j)}\dot{I}^{(l_j)}_{q[\omega_0 t]}(t) &= q_I\big(V^{(l_j)}_{q[\omega_0 t]}(t), V^{(l_j)}_{d[\omega_0 t]}(t), I^{(l_j)}_{q[\omega_0 t]}(t), I^{(l_j)}_{d[\omega_0 t]}(t)\big),\\
\mu_I^{(l_j)}\dot{I}^{(l_j)}_{d[\omega_0 t]}(t) &= d_I\big(V^{(l_j)}_{q[\omega_0 t]}(t), V^{(l_j)}_{d[\omega_0 t]}(t), I^{(l_j)}_{q[\omega_0 t]}(t), I^{(l_j)}_{d[\omega_0 t]}(t)\big),
\end{aligned} \tag{13}$$

where $\mu_V^{(l_j)}$ and $\mu_I^{(l_j)}$ represent time constants of the generic element at bus j; and $q_V\big(\cdot,\cdot,\cdot,\cdot\big)$, $d_V\big(\cdot,\cdot,\cdot,\cdot\big)$, $q_I\big(\cdot,\cdot,\cdot,\cdot\big)$, and $d_I\big(\cdot,\cdot,\cdot,\cdot\big)$ are nonlinear functions of its state variables.

IV. Microgrid reduced-order model 1

Using the singular perturbation techniques discussed in Section II-C, we reduce the order (state-space dimension) of the μHOm described in (11)–(13) to obtain the μROm1.

Assumption IV.1. *For* $\epsilon_1 = 1\times10^{-3}$, *there exists* $k_i^{(j)}$, $\hat{k}^{(i)} \in (0,10)$, $i = 1,2,\ldots,$ *such that:* $\frac{C^{(s_j)}}{\omega_0} = k_1^{(j)}\epsilon_1$, $\frac{L^{(s_j)}}{\omega_0} = k_2^{(j)}\epsilon_1$, $\frac{L_0^{(s_j)}}{\omega_0} = k_3^{(j)}\epsilon_1$, $\mu_V^{(l_j)} = k_4^{(j)}\epsilon_1$, $\mu_I^{(l_j)} = k_5^{(j)}\epsilon_1$, $\frac{1}{\omega_0} = k_6^{(j)}\epsilon_1$, $\frac{1}{\omega_0}\mathbf{L}^{(\boldsymbol{\mathcal{E}})} = diag\left(\hat{k}^{(1)},\ \hat{k}^{(2)},\ \cdots,\ \hat{k}^{(|\mathcal{E}|)}\right)\epsilon_1$.

Assumption IV.2. *The dynamic properties of the μHOm are such that: at each bus j, for*

$$\begin{aligned}
\mathbf{x}_1(t) &= \begin{bmatrix} P_f^{(s_j)}(t) & Q_f^{(s_j)}(t) & \Gamma^{(s_j)}_{q[\alpha^{(j)}(t)]}(t) & \Gamma^{(s_j)}_{d[\alpha^{(j)}(t)]}(t)\end{bmatrix}^{\mathrm{T}},\\
\mathbf{z}_1(t) &= \Big[\delta^{(s_j)}(t) \quad I^{(s_j)}_{q[\omega_0 t]}(t) \quad I^{(s_j)}_{d[\omega_0 t]}(t) \quad \Lambda^{(s_j)}_{[\alpha^{(j)}(t)]}(t)\\
&\quad \hat{E}^{(s_j)}_{q[\omega_0 t]}(t) \quad \hat{E}^{(s_j)}_{d[\omega_0 t]}(t) \quad \Xi^{(s_j)}_{q[\alpha^{(j)}(t)]}(t)\\
&\quad \Xi^{(s_j)}_{d[\alpha^{(j)}(t)]}(t) \quad I^{(l_j)}_{q[\omega_0 t]}(t) \quad I^{(l_j)}_{d[\omega_0 t]}(t)\\
&\quad V^{(l_j)}_{q[\omega_0 t]}(t) \quad V^{(l_j)}_{d[\omega_0 t]}(t) \quad \mathbf{I}^{(\boldsymbol{\mathcal{E}})}_{q[\omega_0 t]}(t) \quad \mathbf{I}^{(\boldsymbol{\mathcal{E}})}_{d[\omega_0 t]}(t)\Big]^{\mathrm{T}},\\
\mathbf{w}_1(t) &= \begin{bmatrix} E^{(s_j)}_{q[\omega_0 t]}(t) & E^{(s_j)}_{d[\omega_0 t]}(t)\end{bmatrix}^{\mathrm{T}},
\end{aligned}$$

the dynamics of $\mathbf{z}_1(t)$ are faster than those of $\mathbf{x}_1(t)$, and the μHOm can be expressed compactly as follows:

$$\begin{aligned}
\dot{\mathbf{x}}_1(t) &= f_1\left(\mathbf{x}_1(t), \mathbf{z}_1(t), \mathbf{w}_1(t), \epsilon_1\right),\\
\epsilon_1\dot{\mathbf{z}}_1(t) &= g_1\left(\mathbf{x}_1(t), \mathbf{z}_1(t), \mathbf{w}_1(t), \epsilon_1\right),\\
\mathbf{0} &= h_1\left(\mathbf{x}_1(t), \mathbf{z}_1(t), \mathbf{w}_1(t), \epsilon_1\right).
\end{aligned} \tag{14}$$

Assumption IV.3. *Equation* (14) *satisfies the conditions for Tikhonov's theorem, as presented in Section II-C.*

Given Assumptions IV.1–IV.3, the μHOm can be reduced to the model,

$$\dot{\bar{\mathbf{x}}}_{0[1]}(t) = f_1\left(\bar{\mathbf{x}}_{0[1]}(t), \zeta_1(\bar{\mathbf{x}}_{0[1]}(t)), \nu_1\left(\bar{\mathbf{x}}_{0[1]}(t), \zeta_1(\bar{\mathbf{x}}_{0[1]}(t))\right), 0\right),$$

which is the so-called Microgrid Reduced-Order Model 1 (μROm1). The explicit ordinary differential equations (ODEs) that constitute μROm1 are derived in Appendix B

V. Microgrid reduced-order model 2

Using the singular perturbation techniques discussed in Section II-C, we reduce the order (state-space dimension) of the μHOm to obtain the μROm2.

Assumption V.1. *For* $\epsilon_2 = 1\times10^{-1}$, *there exists* $k_i^{(j)}$, $\hat{k}^{(i)} \in (0,10)$, $i = 1,2,\ldots,$ *such that:* $\frac{C^{(s_j)}}{\omega_0} = k_1^{(j)}\epsilon_2$, $\frac{L^{(s_j)}}{\omega_0} = k_2^{(j)}\epsilon_2$, $\frac{L_0^{(s_j)}}{\omega_0} = k_3^{(j)}\epsilon_2$, $\mu_V^{(l_j)} = k_4^{(j)}\epsilon_2$, $\mu_I^{(l_j)} = k_5^{(j)}\epsilon_2$, $\frac{1}{\omega_0} = k_6^{(j)}\epsilon_2$, $\frac{1}{\omega_0}\mathbf{L}^{(\boldsymbol{\mathcal{E}})} = diag\left(\hat{k}^{(1)},\ \hat{k}^{(2)},\ \cdots,\ \hat{k}^{(|\mathcal{E}|)}\right)\epsilon_2$, $\frac{2R_0^{(s_j)}+V_{DC}^{(s_j)}K_{P\gamma}^{(s_j)}}{\omega_0 V_{DC}^{(s_j)}K_{I\gamma}^{(s_j)}} = k_5^{(j)}\epsilon_2$.

Assumption V.2. *The dynamic properties of the μHOm are such that: at each bus j, for*

$$\begin{aligned}
\mathbf{x}_2(t) &= \begin{bmatrix} P_f^{(s_j)}(t) & Q_f^{(s_j)}(t)\end{bmatrix}^{\mathrm{T}},\\
\mathbf{z}_2(t) &= \Big[\Gamma^{(s_j)}_{q[\alpha^{(j)}(t)]}(t) \quad \Gamma^{(s_j)}_{d[\alpha^{(j)}(t)]}(t) \quad I^{(s_j)}_{q[\omega_0 t]}(t)\\
&\quad I^{(s_j)}_{d[\omega_0 t]}(t) \quad \hat{E}^{(s_j)}_{q[\omega_0 t]}(t) \quad \hat{E}^{(s_j)}_{d[\omega_0 t]}(t) \quad \Xi^{(s_j)}_{q[\alpha^{(s_j)}(t)]}(t)\\
&\quad \Xi^{(s_j)}_{d[\alpha^{(j)}(t)]}(t) \quad \Lambda^{(s_j)}_{[\alpha^{(j)}(t)]}(t) \quad I^{(l_j)}_{q[\omega_0 t]}(t) \quad I^{(l_j)}_{d[\omega_0 t]}(t)\\
&\quad V^{(l_j)}_{q[\omega_0 t]}(t) \quad V^{(l_j)}_{d[\omega_0 t]}(t) \quad \mathbf{I}^{(\boldsymbol{\mathcal{E}})}_{q[\omega_0 t]}(t) \quad \mathbf{I}^{(\boldsymbol{\mathcal{E}})}_{d[\omega_0 t]}(t) \quad \delta^{(s_j)}(t)\Big]^{\mathrm{T}},\\
\mathbf{w}_2(t) &= \begin{bmatrix} E^{(s_j)}_{q[\omega_0 t]}(t) & E^{(s_j)}_{d[\omega_0 t]}(t)\end{bmatrix}^{\mathrm{T}},
\end{aligned}$$

the dynamics of $\mathbf{z}_2(t)$ are faster than those of $\mathbf{x}_2(t)$, and the μHOm can be expressed compactly as follows:

$$\begin{aligned}
\dot{\mathbf{x}}_2(t) &= f_2\left(\mathbf{x}_2(t), \mathbf{z}_2(t), \mathbf{w}_2(t), \epsilon_2\right),\\
\epsilon_2\dot{\mathbf{z}}_2(t) &= g_2\left(\mathbf{x}_2(t), \mathbf{z}_2(t), \mathbf{w}_2(t), \epsilon_2\right),\\
\mathbf{0} &= h_2\left(\mathbf{x}_2(t), \mathbf{z}_2(t), \mathbf{w}_2(t), \epsilon_2\right).
\end{aligned} \tag{15}$$

Assumption V.3. *Equation* (15) *satisfies the conditions for Tikhonov's theorem, as presented in Section II-C.*

Given Assumptions V.1–V.3, the μHOm can be reduced to the model,

$$\dot{\bar{\mathbf{x}}}_{0[2]}(t) = f_2\left(\bar{\mathbf{x}}_{0[2]}(t), \zeta_2(\bar{\mathbf{x}}_{0[2]}(t)), \nu_2\left(\bar{\mathbf{x}}_{0[2]}(t), \zeta_2(\bar{\mathbf{x}}_{0[2]}(t))\right), 0\right),$$

which is the so-called Microgrid Reduced-Order Model 2 (μROm2). The explicit ODEs that constitute μROm2 are derived in Appendix C

VI. Comparison of UHΦm, μHOm, μROm1 and μROm2

In this section, the time resolution of each reduced-order model is discussed, and for given test cases, the responses of UHΦm, μHOm, μROm1 and μROm2 are compared and validated.

A. Reduced-Model Time Resolution

For formulation of μROmi, where $i = 1, 2$, ϵ_i was chosen such that $\frac{1}{10\epsilon_i}$ represents the largest eigenvalues of the system, associated with the fast states $\mathbf{z}_i(t)$. Consequently, the fast-varying terms in the system response reach steady state in approximately $50\epsilon_i$ seconds and the time resolution of μROmi is $50\epsilon_i$ seconds. Table I shows the time resolution for the reduced-order models.

TABLE I: Reduced-Model Time Resolution

	small parameter	*time-resolution*
μROm1	$\epsilon_1 = 1 \times 10^{-3}$	50 ms
μROm2	$\epsilon_2 = 0.1$	5 s

B. Model Validation

To validate the μHOm, μROm1 and μROm2, the following test case is employed: a grid-feeding inverter connected to an infinite bus through a short transmission line. Using the μHOm, μROm1 and μROm2 respectively, we developed the test case in Simulink. We also designed an ultra-high fidelity model (UHΦm) of the test case on a real-time simulator device called the HIL 402, which was developed by Typhoon HIL [1]. The properties of UHΦm and μHOm are shown in Table II below.

TABLE II: UHΦm vs μHOm

	Parameters	UHΦm	μHOm
LCL Filter	$r_0^{(s_1)}$	0.1Ω	0.1Ω
	$l_0^{(s_1)}$	3mH	3mH
	$r^{(s_1)}$	$1\text{m}\Omega$	$1\text{m}\Omega$
	$l^{(s_1)}$	2μH	2μH
	$\hat{r}_0^{(s_1)}$	$15\text{m}\Omega$	$15\text{m}\Omega$
	$c^{(s_1)}$	20μF	20μF
PWM Inverter	Model	Switched	Averaged
	Rating	35kW	35kW
Current Controller Gains	Proportional	0.015	0.015
	Integral	1	1
PLL	Filter?	Yes	No
	Proportional	100	100
	Integral	3200	3200
	Derivative	1	0
Network	$r^{(e_1)}$	$8\text{m}\Omega$	$8\text{m}\Omega$
	$l^{(e_1)}$	3μH	3μH
∞ Bus Voltage	Magnitude	227V	227V
	Angle	0	0

Firstly, we use a step response analysis to compare the UHΦm, μHOm, μROm1 and μROm2. The simulation starts at $t = 0$, and the system is in steady state with the power references taking values $\boldsymbol{P}_r^{(s_1)} = 12\text{kW}$ and $\boldsymbol{Q}_r^{(s_1)} = 9\text{kW}$. At $t = 0.1\text{s}$, the real power reference is changed instantaneously to $\boldsymbol{P}_r^{(s_1)} = 15\text{kW}$, and at $t = 0.5\text{s}$, the reactive power reference is changed instantaneously to $\boldsymbol{Q}_r^{(s_1)} = 10\text{kW}$. The filtered real and reactive power measurements, $P_f^{(s_1)}(t)$ and $Q_f^{(s_1)}(t)$, are shown in Figs. 2 and 3.

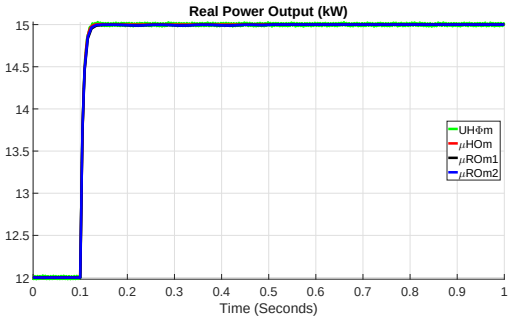

Fig. 2: Real power step response.

Secondly, we present the RegD signal responses of the UHΦm, μHOm, μROm1 and μROm2, for the specified test case. The RegD signal is a normalized dynamic regulation signal developed by PJM interconnection [2] specifically for energy storage devices with limited storage capabilities. The signals are designed to have high gain and short time constants for fast convergence on area control error correction, and to have an energy neutrality integration term [4]. In this analysis, we use a 40 min long RegD test signal that changes every 2 seconds (see [10]). The real power reference, $\boldsymbol{P}_r^{(s_1)}$, is set to the test signal value, and the reactive power reference, $\boldsymbol{Q}_r^{(s_1)}$, is set to zero. The filtered real power

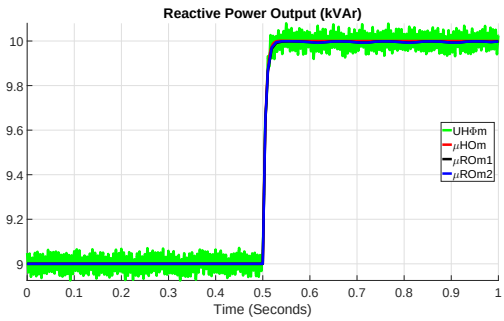

Fig. 3: Reactive power step response.

measurement, $P_f^{(s_1)}(t)$, is shown in Fig. 4, and the normalized root mean square errors of μHOm, μROm1 and μROm2, for $P_f^{(s_1)}(t)$, are shown in Fig. 5

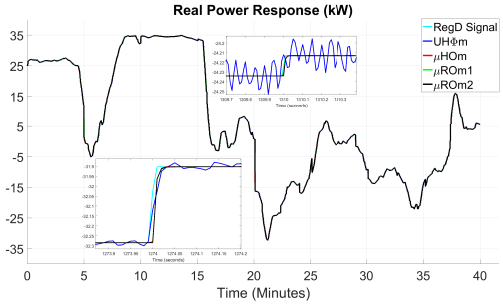

Fig. 4: RegD Test Signal Response

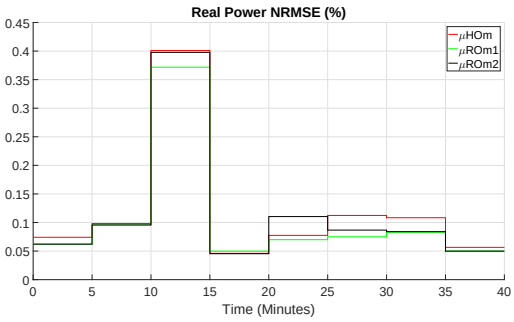

Fig. 5: Normalized Root Mean Square Error (NRMSE)

VII. Conclusion

In this work, we developed a microgrid high-order model (μHOm) by using circuit-theoretic and control laws. We used singular perturbation techniques for model-order reduction of the μHOm, which allowed us to obtain two reduced-order models, μROm1 and μROm2, with the time resolution of each reduced-model identified. We showed that, neglecting the measurement filter dynamics, the μROm1 is a system of differential-algebraic equations, where the dynamic states are the inverter current controller state variables, and the μROm2 is a system of algebraic power balance equations.

We compared the step responses of all three models to that of an Ultra-High Fidelity model for the microgrid, designed to mimic a real system. Using the time resolutions to analyze each models response, we observed that the step responses of μHOm, μROm1 and μROm2 track the averaged step response of the UHΦm. This is due to the inverter averaged model, used to develop μHOm. The real power responses to a RegD signal test case were also presented, with the normalized root mean square error for all models shown to be less than 0.5 percent.

Appendix A
Reduction of Equations for the LCL Filter, PLL, Network and Generic Element

Assumption A.1. *The generic model in* (13) *can be reduced to the so called ZIP model (see e.g. [13]), given by:*

$$\begin{aligned} V_{q[\omega_0 t]}^{(l_j)}(t) I_{q[\omega_0 t]}^{(l_j)}(t) + V_{d[\omega_0 t]}^{(l_j)}(t) I_{d[\omega_0 t]}^{(l_j)}(t) = & -P_0^{(l_j)} - \left|\vec{\mathbf{V}}^{(l_j)}(t)\right| P_1^{(l_j)} \\ & - \left|\vec{\mathbf{V}}^{(l_j)}(t)\right|^2 P_2^{(l_j)}, \\ V_{q[\omega_0 t]}^{(l_j)}(t) I_{d[\omega_0 t]}^{(l_j)}(t) - V_{d[\omega_0 t]}^{(l_j)}(t) I_{q[\omega_0 t]}^{(l_j)}(t) = & -Q_0^{(l_j)} - \left|\vec{\mathbf{V}}^{(l_j)}(t)\right| Q_1^{(l_j)} \\ & - \left|\vec{\mathbf{V}}^{(l_j)}(t)\right|^2 Q_2^{(l_j)}, \end{aligned}$$

where $P_0^{(l_j)}$, $P_1^{(l_j)}$, $P_2^{(l_j)}$, $Q_0^{(l_j)}$, $Q_1^{(l_j)}$ *and* $Q_2^{(l_j)}$ *denote constants for the element at bus* j*, and* $\left|\vec{\mathbf{V}}^{(l_j)}(t)\right|$ *denotes the phasor magnitude of* $V_{q[\omega_0 t]}^{(l_j)}(t) - \mathrm{j} V_{d[\omega_0 t]}^{(l_j)}(t)$.

Let $\hat{\theta}^{(s_j)}(t) := \arctan\left(\frac{-E_{d[\omega_0 t]}^{(s_j)}(t)}{E_{q[\omega_0 t]}^{(s_j)}(t)}\right)$, and $\theta^{(l_j)}(t) := \arctan\left(\frac{-V_{d[\omega_0 t]}^{(l_j)}(t)}{V_{q[\omega_0 t]}^{(l_j)}(t)}\right)$. Let $\beta^{(j)} \in \{0,1\}$ be a constant such that $\beta^{(j)} = 1$ if bus $j \in \mathcal{V}_{\mathcal{I}}$, and $\beta^{(j)} = 0$ otherwise. Also, let

$$\begin{aligned} \left|\vec{\mathbf{V}}^{(e_m)}(t)\right| &= \left|\vec{\mathbf{V}}^{(l_j)}(t)\right| \left|\vec{\mathbf{V}}^{(l_k)}(t)\right|, \\ \text{at bus } j: \quad \theta^{(e_m)}(t) &= \theta^{(l_j)}(t) - \theta^{(l_k)}(t), \\ \text{at bus } k: \quad \theta^{(e_m)}(t) &= \theta^{(l_k)}(t) - \theta^{(l_j)}(t). \end{aligned}$$

Setting $\epsilon_1 = 0$ and $\epsilon_2 = 0$ in (14) and (15), the LCL filter, PLL, network and generic element models can be reduced to a nonlinear system of power balance equations.

Assumption A.2. *The jacobian of the nonlinear system of power balance equations is invertible in the domain of interest.*

APPENDIX B
THE μROM1

Based on Assumptions IV.1–IV.3, the explicit ODEs that constitute μROm1 are given as follows:

At each bus $j \in \mathcal{V}_{\mathcal{I}}$,

$$\frac{2R_0^{(s_j)}+V_{DC}^{(s_j)}K_{P\gamma}^{(s_j)}}{\omega_0 V_{DC}^{(s_j)}K_{I\gamma}^{(s_j)}}\frac{d\Gamma^{(s_j)}_{q[\alpha^{(j)}(t)]}(t)}{dt}=-\Gamma^{(s_j)}_{q[\alpha^{(j)}(t)]}(t)+\frac{2R_0^{(s_j)}}{V_{DC}^{(s_j)}K_{I\gamma}^{(s_j)}}\frac{\boldsymbol{P}_r^{(s_j)}}{\left|\vec{\mathbf{E}}^{(s_j)}(t)\right|},$$

$$\frac{2R_0^{(s_j)}+V_{DC}^{(s_j)}K_{P\gamma}^{(s_j)}}{\omega_0 V_{DC}^{(s_j)}K_{I\gamma}^{(s_j)}}\frac{d\Gamma^{(s_j)}_{d[\alpha^{(j)}(t)]}(t)}{dt}=-\Gamma^{(s_j)}_{d[\alpha^{(j)}(t)]}(t)+\frac{2R_0^{(s_j)}}{V_{DC}^{(s_j)}K_{I\gamma}^{(s_j)}}\frac{\boldsymbol{Q}_r^{(s_j)}}{\left|\vec{\mathbf{E}}^{(s_j)}(t)\right|}.$$

Let $\boldsymbol{E}(j)$ represent the set of edges incident to node j such that $e_m \in \boldsymbol{E}(j)$ if and only if the edge e_m is incident to node j. The power balance equations at bus $j \in \mathcal{V}$ are given by:

$$\begin{aligned}
0=&-\frac{\beta^{(j)}V_{DC}^{(s_j)}\left(K_{I\gamma}^{(s_j)}\left|\vec{\mathbf{E}}^{(s_j)}(t)\right|\Gamma^{(s_j)}_{q[\alpha^{(j)}(t)]}(t)+K_{P\gamma}^{(s_j)}\boldsymbol{P}_r^{(s_j)}\right)}{\left(2R_0^{(s_j)}+V_{DC}^{(s_j)}K_{P\gamma}^{(s_j)}\right)}\\
&+\beta^{(j)}\hat{G}^{(s_j)}\left|\vec{\mathbf{E}}^{(s_j)}(t)\right|^2+\beta^{(j)}G^{(s_j)}\left|\vec{\mathbf{E}}^{(s_j)}(t)\right|^2\\
&-\beta^{(j)}\left|\vec{\mathbf{E}}^{(s_j)}(t)\right|\left|\vec{\mathbf{V}}^{(l_j)}(t)\right|\Big(G^{(s_j)}\cos\left(\hat{\theta}^{(s_j)}(t)-\theta^{(l_j)}(t)\right)\\
&+\beta^{(j)}B^{(s_j)}\sin\left(\hat{\theta}^{(s_j)}(t)-\theta^{(l_j)}(t)\right)\Big),\\
0=&-\frac{\beta^{(j)}V_{DC}^{(s_j)}\left(K_{I\gamma}^{(s_j)}\left|\vec{\mathbf{E}}^{(s_j)}(t)\right|\Gamma^{(s_j)}_{d[\alpha^{(j)}(t)]}(t)+K_{P\gamma}^{(s_j)}\boldsymbol{Q}_r^{(s_j)}\right)}{\left(2R_0^{(s_j)}+V_{DC}^{(s_j)}K_{P\gamma}^{(s_j)}\right)}\\
&-\beta^{(j)}\hat{B}^{(s_j)}\left|\vec{\mathbf{E}}^{(s_j)}(t)\right|^2-\beta^{(j)}B^{(s_j)}\left|\vec{\mathbf{E}}^{(s_j)}(t)\right|^2\\
&-\beta^{(j)}\left|\vec{\mathbf{E}}^{(s_j)}(t)\right|\left|\vec{\mathbf{V}}^{(l_j)}(t)\right|\Big(G^{(s_j)}\sin\left(\hat{\theta}^{(s_j)}(t)-\theta^{(l_j)}(t)\right)\\
&-\beta^{(j)}B^{(s_j)}\cos\left(\hat{\theta}^{(s_j)}(t)-\theta^{(l_j)}(t)\right)\Big),\\
0=&\,P_0^{(l_j)}+\left|\vec{\mathbf{V}}^{(l_j)}(t)\right|P_1^{(l_j)}+\left|\vec{\mathbf{V}}^{(l_j)}(t)\right|^2P_2^{(l_j)}+\beta^{(j)}G^{(s_j)}\left|V^{(l_j)}(t)\right|^2\\
&-\beta^{(j)}\left|\vec{\mathbf{V}}^{(l_j)}(t)\right|\left|\vec{\mathbf{E}}^{(s_j)}(t)\right|\Big(G^{(s_j)}\cos\left(\theta^{(l_j)}(t)-\hat{\theta}^{(s_j)}(t)\right)\\
&+B^{(s_j)}\sin\left(\theta^{(l_j)}(t)-\hat{\theta}^{(s_j)}(t)\right)\Big)+\left|\vec{\mathbf{V}}^{(l_j)}(t)\right|^2\sum_{e_m\in\boldsymbol{E}(j)}G^{(e_m)}\\
&-\sum_{e_m\in\boldsymbol{E}(j)}\left|\vec{\mathbf{V}}^{(e_m)}(t)\right|\Big(G^{(e_m)}\cos\left(\theta^{(e_m)}(t)\right)+B^{(e_m)}\sin\left(\theta^{(e_m)}(t)\right)\Big),\\
0=&\,Q_0^{(l_j)}+\left|\vec{\mathbf{V}}^{(l_j)}(t)\right|Q_1^{(l_j)}+\left|\vec{\mathbf{V}}^{(l_j)}(t)\right|^2Q_2^{(l_j)}-\beta^{(j)}B^{(l_j)}\left|\vec{\mathbf{V}}^{(l_j)}(t)\right|^2\\
&-\beta^{(j)}\left|\vec{\mathbf{V}}^{(l_j)}(t)\right|\left|\vec{\mathbf{E}}^{(s_j)}(t)\right|\Big(G^{(s_j)}\sin\left(\theta^{(l_j)}(t)-\hat{\theta}^{(s_j)}(t)\right)\\
&-B^{(s_j)}\cos\left(\theta^{(l_j)}(t)-\hat{\theta}^{(s_j)}(t)\right)\Big)-\left|\vec{\mathbf{V}}^{(l_j)}(t)\right|^2\sum_{e_m\in\boldsymbol{E}(j)}B^{(e_m)}\\
&-\sum_{e_m\in\boldsymbol{E}(j)}\left|\vec{\mathbf{V}}^{(e_m)}(t)\right|\Big(G^{(e_m)}\sin\left(\theta^{(e_m)}(t)\right)\;-B^{(e_m)}\cos\left(\theta^{(e_m)}(t)\right)\Big).
\end{aligned}$$

where

$\hat{G}^{(s_j)}=\frac{\hat{R}_0^{(s_j)}}{\left(\hat{R}_0^{(s_j)}\right)^2+\left(\frac{1}{C^{(s_j)}}\right)^2}$, $\hat{B}^{(s_j)}=\frac{C^{(s_j)}}{\left(C^{(s_j)}\hat{R}_0^{(s_j)}\right)^2+1}$, $G^{(s_j)}=\frac{R^{(s_j)}}{\left(R^{(s_j)}\right)^2+\left(L^{(s_j)}\right)^2}$, $B^{(s_j)}=\frac{-L^{(s_j)}}{\left(R^{(s_j)}\right)^2+\left(L^{(s_j)}\right)^2}$, $G^{(e_m)}=\frac{R^{(e_m)}}{\left(R^{(e_m)}\right)^2+\left(L^{(e_m)}\right)^2}$, and $B^{(e_m)}=\frac{-L^{(e_m)}}{\left(R^{(e_m)}\right)^2+\left(L^{(e_m)}\right)^2}$. The filtered real and reactive power measurements, $P_f^{(s_j)}(t)$ and $Q_f^{(s_j)}(t)$, can be described by:

$$\begin{aligned}
\frac{1}{\omega_c^{(s_j)}}\frac{dP_f^{(s_j)}(t)}{dt}=&-P_f^{(s_j)}(t)+E^{(s_j)}_{q[\omega_0 t]}(t)I^{(s_j)}_{q[\omega_0 t]}(t)+E^{(s_j)}_{d[\omega_0 t]}(t)I^{(s_j)}_{d[\omega_0 t]}(t),\\
\frac{1}{\omega_c^{(s_j)}}\frac{dQ_f^{(s_j)}(t)}{dt}=&-Q_f^{(j)}(t)+E^{(s_j)}_{q[\omega_0 t]}(t)I^{(s_j)}_{d[\omega_0 t]}(t)-E^{(s_j)}_{d[\omega_0 t]}(t)I^{(s_j)}_{q[\omega_0 t]}(t),
\end{aligned}$$

with $\omega_c^{(s_j)}$ denoting the filter cut-off frequency.

APPENDIX C
THE μROM2

Based on Assumptions V.1–V.3, the explicit ODEs that constitute μROm2 are given as follows:

Let $\boldsymbol{E}(j)$ represent the set of edges incident to node j such that $e_m \in \boldsymbol{E}(j)$ if and only if the edge e_m is incident to node j. At each bus $j \in \mathcal{V}$,

$$\begin{aligned}
0=&-\beta^{(j)}\boldsymbol{P}_r^{(s_j)}+\beta^{(j)}\hat{G}^{(s_j)}\left|\vec{\mathbf{E}}^{(s_j)}(t)\right|^2+\beta^{(j)}G^{(s_j)}\left|\vec{\mathbf{E}}^{(s_j)}(t)\right|^2\\
&-\beta^{(j)}\left|\vec{\mathbf{E}}^{(s_j)}(t)\right|\left|\vec{\mathbf{V}}^{(l_j)}(t)\right|\Big(G^{(s_j)}\cos\left(\hat{\theta}^{(s_j)}(t)-\theta^{(l_j)}(t)\right)\\
&+\beta^{(j)}B^{(s_j)}\sin\left(\hat{\theta}^{(s_j)}(t)-\theta^{(l_j)}(t)\right)\Big),\\
0=&-\beta^{(j)}\boldsymbol{Q}_r^{(s_j)}-\beta^{(j)}\hat{B}^{(s_j)}\left|\vec{\mathbf{E}}^{(s_j)}(t)\right|^2-\beta^{(j)}B^{(s_j)}\left|\vec{\mathbf{E}}^{(s_j)}(t)\right|^2\\
&-\beta^{(j)}\left|\vec{\mathbf{E}}^{(s_j)}(t)\right|\left|\vec{\mathbf{V}}^{(l_j)}(t)\right|\Big(G^{(s_j)}\sin\left(\hat{\theta}^{(s_j)}(t)-\theta^{(l_j)}(t)\right)\\
&-\beta^{(j)}B^{(s_j)}\cos\left(\hat{\theta}^{(s_j)}(t)-\theta^{(l_j)}(t)\right)\Big),\\
0=&\,P_0^{(l_j)}+\left|\vec{\mathbf{V}}^{(l_j)}(t)\right|P_1^{(l_j)}+\left|\vec{\mathbf{V}}^{(l_j)}(t)\right|^2P_2^{(l_j)}+\beta^{(j)}G^{(s_j)}\left|V^{(l_j)}(t)\right|^2\\
&-\beta^{(j)}\left|\vec{\mathbf{V}}^{(l_j)}(t)\right|\left|\vec{\mathbf{E}}^{(s_j)}(t)\right|\Big(G^{(s_j)}\cos\left(\theta^{(l_j)}(t)-\hat{\theta}^{(s_j)}(t)\right)\\
&+B^{(s_j)}\sin\left(\theta^{(l_j)}(t)-\hat{\theta}^{(s_j)}(t)\right)\Big)+\left|\vec{\mathbf{V}}^{(l_j)}(t)\right|^2\sum_{e_m\in\boldsymbol{E}(j)}G^{(e_m)}\\
&-\sum_{e_m\in\boldsymbol{E}(j)}\left|\vec{\mathbf{V}}^{(e_m)}(t)\right|\Big(G^{(e_m)}\cos\left(\theta^{(e_m)}(t)\right)+B^{(e_m)}\sin\left(\theta^{(e_m)}(t)\right)\Big),\\
0=&\;Q_0^{(l_j)}+\left|\vec{\mathbf{V}}^{(l_j)}(t)\right|Q_1^{(l_j)}+\left|\vec{\mathbf{V}}^{(l_j)}(t)\right|^2Q_2^{(l_j)}-\beta^{(j)}B^{(l_j)}\left|\vec{\mathbf{V}}^{(l_j)}(t)\right|^2\\
&-\beta^{(j)}\left|\vec{\mathbf{V}}^{(l_j)}(t)\right|\left|\vec{\mathbf{E}}^{(s_j)}(t)\right|\Big(G^{(s_j)}\sin\left(\theta^{(l_j)}(t)-\hat{\theta}^{(s_j)}(t)\right)\\
&-B^{(s_j)}\cos\left(\theta^{(l_j)}(t)-\hat{\theta}^{(s_j)}(t)\right)\Big)-\left|\vec{\mathbf{V}}^{(l_j)}(t)\right|^2\sum_{e_m\in\boldsymbol{E}(j)}B^{(e_m)}\\
&-\sum_{e_m\in\boldsymbol{E}(j)}\left|\vec{\mathbf{V}}^{(e_m)}(t)\right|\Big(G^{(e_m)}\sin\left(\theta^{(e_m)}(t)\right)\;-B^{(e_m)}\cos\left(\theta^{(e_m)}(t)\right)\Big).
\end{aligned}$$

where

$\hat{G}^{(s_j)}=\frac{\hat{R}_0^{(s_j)}}{\left(\hat{R}_0^{(s_j)}\right)^2+\left(\frac{1}{C^{(s_j)}}\right)^2}$, $\hat{B}^{(s_j)}=\frac{C^{(s_j)}}{\left(C^{(s_j)}\hat{R}_0^{(s_j)}\right)^2+1}$, $G^{(s_j)}=\frac{R^{(s_j)}}{\left(R^{(s_j)}\right)^2+\left(L^{(s_j)}\right)^2}$, $B^{(s_j)}=\frac{-L^{(s_j)}}{\left(R^{(s_j)}\right)^2+\left(L^{(s_j)}\right)^2}$, $G^{(e_m)}=\frac{R^{(e_m)}}{\left(R^{(e_m)}\right)^2+\left(L^{(e_m)}\right)^2}$, and $B^{(e_m)}=\frac{-L^{(e_m)}}{\left(R^{(e_m)}\right)^2+\left(L^{(e_m)}\right)^2}$. The filtered real and reactive

power measurements, $P_f^{(s_j)}(t)$ and $Q_f^{(s_j)}(t)$, can be described by:

$$\frac{1}{\omega_c^{(s_j)}}\frac{dP_f^{(s_j)}(t)}{dt} = -P_f^{(s_j)}(t) + E_{q[\omega_0 t]}^{(s_j)}(t)I_{q[\omega_0 t]}^{(s_j)}(t) + E_{d[\omega_0 t]}^{(s_j)}(t)I_{d[\omega_0 t]}^{(s_j)}(t),$$
$$\frac{1}{\omega_c^{(s_j)}}\frac{dQ_f^{(s_j)}(t)}{dt} = -Q_f^{(j)}(t) + E_{q[\omega_0 t]}^{(s_j)}(t)I_{d[\omega_0 t]}^{(s_j)}(t) - E_{d[\omega_0 t]}^{(s_j)}(t)I_{q[\omega_0 t]}^{(s_j)}(t),$$

with $\omega_c^{(s_j)}$ denoting the filter cut-off frequency.

REFERENCES

[1] Typhoon HIL. URL https://www.typhoon-hil.com/.

[2] Pennsylvania New Jersey Maryland Interconnection LLC (Mid-Atlantic region power pool). URL http://www.pjm.com/.

[3] S. Anand and B. G. Fernandes. Reduced-order model and stability analysis of low-voltage dc microgrid. *IEEE Transactions on Industrial Electronics*, 60(11):5040–5049, Nov. 2013.

[4] S. Benner. A brief history of regulation signals at pjm, Jun 2014. URL http://www.pjm.com/~/media/committees-groups/committees/oc/20150701-rpi/20150701-item-02-history-of-regulation-d.ashx.

[5] A.R. Bergen and V. Vittal. *Power Systems Analysis*. Prentice Hall, 2000.

[6] J. H. Chow. *Time-Scale Modeling of Dynamic Networks with Applications to Power Systems*. Springer-Verlag, 1982.

[7] K. Kodra, Ningfan Zhong, and Z. Gajić. Model order reduction of an islanded microgrid using singular perturbations. In *Proc. of American Control Conference, pp. 3650-3655, Chicago, IL, 2016*.

[8] P. Kokotović, H. K. Khalil, and J. O'Reilly. *Singular Perturbation Methods in Control: Analysis and Design*. Classics in Applied Mathematics. Society for Industrial and Applied Mathematics, 1986.

[9] P.C. Krause, O. Wasynczuk, S.D. Sudhoff, S. Pekarek, Institute of Electrical, and Electronics Engineers. *Analysis of Electric Machinery and Drive Systems*. IEEE Press Series on Power Engineering. Wiley, 2013.

[10] PJM. Normalized signal test: Regd, Aug 2014. URL http://www.pjm.com/~/media/markets-ops/ancillary/regd-test-wave.ashx.

[11] N. Pogaku, M. Prodanovic, and T. C. Green. Modeling, analysis and testing of autonomous operation of an inverter-based microgrid. *IEEE Transactions on Power Electronics*, 22(2):613–625, Mar. 2007.

[12] M. Rasheduzzaman, J. A. Mueller, and J. W. Kimball. Reduced-order small-signal model of microgrid systems. *IEEE Transactions on Sustainable Energy*, 6(4):1292–1305, Oct. 2015.

[13] P.W. Sauer and A. Pai. *Power System Dynamics and Stability*. Stipes Publishing L.L.C., 2006.

[14] J. Schiffer, D. Zonetti, R. Ortega, A. M. Stankovic, T. Sezi, and J. Raisch. Modeling of microgrids - from fundamental physics to phasors and voltage sources. *CoRR*, abs/1505.00136, May 2015.

[15] A. Yazdani and R. Iravani. *Voltage-Sourced Converters in Power Systems*. Wiley, Jan. 2010.